Characterization of methane inverse diffusion flames in a multi-slot burner

Miguel Filipe Neves Ribeiro
miguel.n.ribeiro@ist.utl.pt

Instituto Superior Técnico, Universidade de Lisboa, Portugal

June 2019

Abstract

Inverse diffusion flames (IDF), present several potentially advantageous characteristics towards the goal of controlling noxious emissions and achieving a higher efficiency. Combining benefits of a premixed and diffusion flame, IDF have shown an extended lean flammability range and a smaller production of NO_x and soot than a normal diffusion flame while simultaneously avoiding flashback. A complete methane IDF range in a multi-slot burner was established, from pure diffusion regime to a global equivalence ratio of 0.2. Chemiluminescence spectroscopy was utilized to measure local ϕ values and PIV was applied to obtain the velocity vector maps of each flame type, a number of velocity measurements were made at different flame heights and at their flowrate-equivalent isothermal cases. Permitting a comparison between the isothermal and flame cases and the study of the flame velocity profile evolution. For the established IDF flame range four different flame types were identified, of which three, Type II, III and IV were studied more in depth with the previously mentioned techniques. Accentuated morphology transformations were verified, from a dual-regime, resembling a soot producing partial premixed flame to a totally blue open top flame with intense upstream mixing. The air-fuel velocity ratio (V_r) was found to be an important governing parameter in the definition of the flame structures, due to its role in the air-fuel jet mixing. The neck structure characteristic of flame type IV was formed at $Re_{air} = 355$, functioning as a structural stabilization mechanism, presenting a recirculation zone due to the high pressure around the impingement stagnation point.
Keywords: Inverse diffusion flame, chemiluminescence, spectroscopy, particle image velocimetry, slot burner, morphology

1. Introduction

As societies evolved, their priorities were naturally ever-changing, at the turn of the century combustion saw tremendous advancements, from engines including the first plans for gas turbines, to the development of coal power plants. We had the future on our sights and the pace was tremendous, our dependency on these kinds of technology was well underway.

Although we were granted with a greatly improved quality of living, given to us not only by electricity generated with combustion but also its various other applications. This was not to be without a drawback, and so the environmental issues were ushered on, the damage demanded a rapid focus towards the development of new and improved technologies and applications of combustion that have the reduction and control of the emission of pollutants, combined with achieving higher energetic efficiency, as the central goal.

Nowadays there is an ongoing research effort focused on controlling three of the more dangerous pollutants emitted in combustion, CO, CO_2 and NO_x. This pushed developments towards leaner and colder flames, approaching the problem of flame stabilization within the parameters most ideal to minimize the emission of these noxious components. Inverse diffusion flames were initially investigated due to their potential in presenting several advantageous characteristics to achieve this desired behavior, a combination of a premixed flame and a diffusion flame that can have a larger flammability range than a premixed flame while also potentially producing less NO_x and soot than a normal diffusion flame (NDF). This type of flames has great interest for application in industrial and domestic heating processes, therefore further research on this topic is valuable

The vast majority of research and literature on diffusion flames has been devoted to normal flame configurations, where there is an environment of excess air surrounding the burning fuel. However, the research efforts into the inverse configuration have recently increased. One of the first substantial

studies regarding this configuration was presented in 1985 by Wu and Essenhigh [1]. A thorough investigation was performed in order to identify the structure of laminar methane IDFs stabilized in a simple coaxial burner, with an approach based on visual appearance and air-fuel velocities. Six different regimes were identified along with the predicted temperature and stable species profiles, pointing to a nearly indistinguishable mathematical similarity between IDF and NDF. From this defining study two similar flames were shown to be the most representative of IDF, accounting for more than 50% of the flame map. These flames presented a parabolic blue combustion zone, with a yellow zone starting about 1/3 of the way up, forming a tapered truncated annulus with an open top and a shorter visual flame height in comparison with NDF.

At this stage a third characterizing parameter for IDF (in addition to the previously mentioned air and fuel velocities) was starting to be widely used, the global equivalence ratio (ϕ_g). This quantity was directly adapted from the commonly utilized equivalence ratio (ϕ) for premixed flames, defined as the ratio between the fuel-to-oxidizer ratio and the stoichiometric fuel-to-oxidizer ratio. The use of this parameter in diffusion flames does not directly translate to a rich or lean mixture as in the premixed case, functioning only as an indicative reference measure of the air and fuel quantities that are being input into the burner separately.

All the previously mentioned studies utilized a co-annular (CoA) burners, with an interior air channel and a surrounding concentric annular air channel, as depicted in Figure 1(a). A second important burner configuration saw a comprehensive research effort to improve flame stability and mixing characteristics. The circumferential arranged ported burner (CAP) can be seen as a special case of traditional IDF, where the annular fuel jet is subdivided into multiple surrounding jets in a circumference centered on the singular central air jets as shown in Figure 1(b).

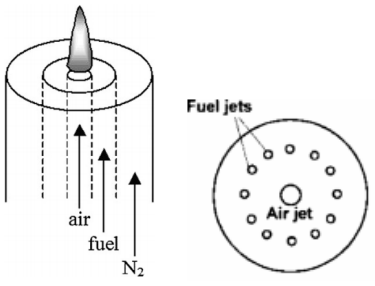

(a) CoA burner; Source: [2] (b) CAP burner; Source: [3]

Figure 1: Main burner configurations

Focusing now on the approaches more closely related to the present study, in particular the use of multi slit burners, two relevant studies have been undertaken utilizing this burner configuration, where the two concentric channels (oxidizer and surrounding fuel) are substituted by a central rectangular air slit with two adjacent parallel fuel slits. Shaddix et al. [4] focused on a comparative analysis between normal and inverse diffusion flames for this particular burner geometry at very specific flow rates, identifying the inversion in OH and policyclic aromatic hydrocarbons (PAH, these are formed in incomplete combustion and are associated with soot production) Laser-Induced-Fluorescence (LIF) layer positioning for both methane and ethylene flames. Furthermore IDF were found relatively unstable in comparison to the NDF.

In summary, most of the work concerning IDF has focused on flame appearance and structure, flame height, temperature profiles, soot formation characteristics and emissions for mainly CoA and CAP style burners.

1.1. Objectives

The present work intends to study and characterize methane inverse diffusion flames (IDF) in a multi-slot burner. For this purpose it was set out to experimentally obtain a complete global equivalence ratio (ϕ_g) working range of methane IDF for two particular flame powers (fixed fuel flow rate). This was carried out through the central air flow rate variation. Characteristic flame types are to be analyzed utilizing two particular techniques: flame photography with visual analysis, chemiluminescence spectroscopy and particle image velocimetry (PIV).

The combination of these three techniques will hopefully allow for a quite good methodological structure to characterize the flame morphologies. Flame range photography for the preliminary interest structure identification and the effects of key parameter variations. The chemiluminescence spectroscopy will permit a more detailed measurement of the local equivalence ratio (ϕ), which is particularly useful to understand the mixing phenomena for this type of flame, where the local ϕ are expected to be quite intense due to its inherent diffusive nature. And finally the velocity mappings obtained through PIV will function as an additional window into the inter-jet flow mixing dynamics, isothermal and flame comparisons and also flame velocity profile evolutions.

2. Background

General Setup

A schematic of the experimental setup used in this work is displayed in Figure 2. To guarantee a proper control of pressure, temperature and volu-

metric flowrate each fuel line was assigned a dedicated mass flow meter. Methane is introduced into the system from a gas canister, and divided into two separate streams feeding into two digital *Alicat Mass Flow Controllers* with a maximum capacity of 5 SLPM[1] each, Air was introduced through a dedicated line and passed through an air filter in order to remove the water and other impurities before being fed into a third *Alicat Mass Flow Controller* with a maximum capacity of 50 SLPM. All control was done utilizing a *LabView* interface.

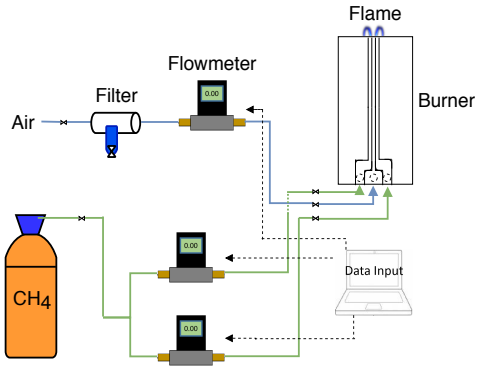

Figure 2: Experimental Setup Schematic

Burner Characterization
For the purposes of this work, a two dimensional slit burner with rectangular channels was utilized. In order to characterize IDF under various conditions, this burner was equipped with four 1 mm thick AISI Type 304 Stainless Steel plates .This configuration was chosen to ensure a proper flow development at the burner outlet, which proved quite unstable with a preliminary configuration with converging interior channels and a shorter constant section. The burner has a height of 350 mm, 38 mm slit length and a slit width of 2 mm for all three channels, with a slightly larger injection chamber for both fuel channels due to geometric constraints.

Establishing flame range and parameters
The chosen procedure for the establishment of the flame range subject to analysis, was based on the more prevalent approaches on the study of IDF, as can be seen on a number of the most relevant and recent works [5, 6, 7, 8, 9]. A specific flame characteristic is predominantly utilized, the equivalence ratio (ϕ), which defines the global ratio between the fuel-to-oxidizer ratio and the stoichiometric fuel-to-oxidizer ratio. It is important though, to bear in mind that this parameter while with clear significance in characterizing premixed flames, where there is a homogeneous mixture of fuel and oxidizer with a determinate ratio. However, it should not be interpreted in the same manner regarding diffusion flames, or for this matter IDF, as the ratio between fuel and oxidizer will be highly variable locally, ranging from regions with 100% to 0% fuel and a stoichiometric flame front reaction center line.

Therefore, for clarity, the equivalence ratio will be denominated as ϕ_g, and interpreted as a global reference based on the input fuel and oxidizer flow rates as defined in Equation 1.

$$\phi_g = \frac{\frac{n_{fuel}}{n_{air}}}{\left(\frac{n_{fuel}}{n_{air}}\right)_{stoich}} \tag{1}$$

Where $\frac{n_{fuel}}{n_{air}}$ is the actual molar fuel-to-oxidizer ratio and $\left(\frac{n_{fuel}}{n_{air}}\right)_{stoich}$ is the molar stoichiometric fuel-to-oxidizer ratio.

Another important parameter utilized for the flame range characterization was the velocity ratio (Equation 2), providing a more immediate perception of the velocities involved and their possible mixing mechanisms and interactions.

$$V_r = \frac{V_{air}}{V_{fuel}} \tag{2}$$

To properly discern the affecting variables, and maintain a flame dimension adequate for visualization, a fixed fuel flow approach was undertaken [10, 8, 2]. Two specific fuel flow rates were fixed, corresponding to a flame power of 238 W and 455 W.

2.1. Chemiluminescence Spectroscopy

In order to adequately understand and characterize the chemical kinetics in play, an optical technique based on flame chemiluminescence was utilized. This technique is based on the spontaneous emission of electromagnetic radiation from the chemical reactions occurring in the combustion process. As an excited radical formed in a reaction goes to its ground state, the emitted radiation will have a specific wavelength and intensity which can be correlated to different flame properties intrinsically related to the setup [11, 12].

Experimental Setup and Procedure

The setup utilized was composed of a light collecting system consisting of an optical probe arranged with three degrees of freedom in order to adequately adjust the distance to the flame and the sweeping of the flame fronts. A *QP-400-2-SR-BX* optical fiber from *Ocean Optics*, model with a core diameter of $400 \pm 4\mu$m and a solid angle of 25^o, was attached to the spectrometer. The optical probe setup was designed for the collection of light emission in a

[1] standard liter per minute

cylindrical volume aligned with the slits and the two dimensional flames, as depicted in schematic of Figure 3.

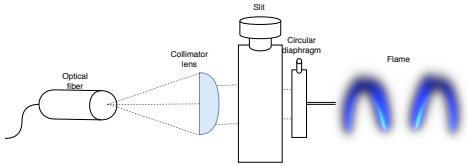

(a) Probe Schematic

Figure 3: Probing Setup.

To do so a collimator lens and two adjustable diaphragms were coupled to the optical fiber, an horizontal slit followed by a circular diaphragm, this way it was possible to limit the area under analysis to a diameter of 0.2mm controlling the amount of light entering the fiber and the spatial resolution. The acquired signal was received by an *Ocean Optics QE65000 Spectrophotometer* with a 200 to 1100 nm wavelength range and the incoming signal ultimately processed by a computer running the *SpectraSuite* software.

System Calibration

To correlate the measured values of radical intensity, acquired throughout the chemiluminescence technique to the equivalence ratio, a calibration procedure is essential. Its main goal is to determine an adequate correlation through the analysis of a the radical radiation emissions of a reference flame with a known equivalence ratio.

As a reference setup, the same slot burner was utilized in a single slot premixed configuration of air and methane as to guarantee a known input of equivalence ratio and power. The various radical ratios obtained throughout the whole equivalence ratio under analysis exhibit varying sensitivities to ϕ along its range. Bearing this in mind, the optimum calibration will be a composition of the partial ideal working ranges of each ratio, represented in Figure 4.

2.2. Particle Image Velocimetry

Particle-image-velocimetry (PIV) is a quantitative velocity measuring technique. It offers valuable advantages when compared to traditional flow measurement techniques such as the Doppler velocimetry and hot-wire anemometry due to its precision and non-intrusive nature. The flow is undisturbed by probes allowing for a whole-field measurement of the velocity [13, 14].

This technique utilizes small tracer particles inserted in the flow which are subsequently illuminated using a double pulsed laser in the area of interest to produce a green light planar sheet with

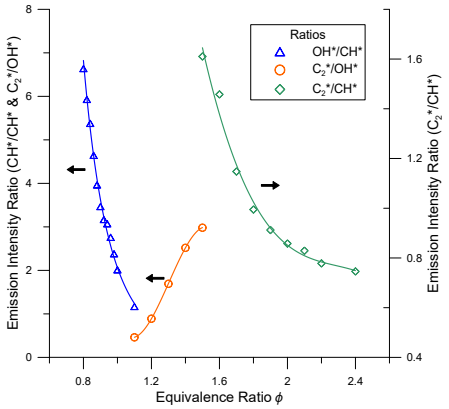

Figure 4: Final combined ϕ calibration.

a wavelength of 530 nm. This laser is synchronized with a high-speed sCMOS camera using a synchronizer connected to the central acquisition system. The camera will acquire two consecutive frames of laser-illuminated particles embedded in the flow under study. The two-dimensional velocity field can then be determined by cross-correlating the two consecutive frames, as well as the time interval between laser pulses and the distance traveled by the seeding particles.

Experimental Setup and Procedure

The setup utilized consisted of five main components: the double pulsed laser, a *Dantec Dual Power 65-15 Yag* with two laser cavities with a maximum laser pulse frequency of 15 Hz each and a wavelength of 532 nm; the image acquisition system, provided by a *HiSense Zyla sCMOS* camera with a framerate of 40 FPS and a resolution of 2560 x 2160 pixels and an added 532 nm filter to protect the camera CCDs and better define the particle light scattering within the flame itself. The synchronization between these two components was handled by a *BNC 575 Series Pulse Generator*, controlled centrally by an acquisition system on a dedicated computer utilizing the *Dantec DynamicStudio* software

The final component is the seeding system, this setup in particular used 3 separate independent seeding bottles with *Logitech 5 micron Calcinated Aluminium Oxide Powder* particles, in order to assure an adequate and uniform particle density in each channel, in spite of the different flow rates. Two independent electromagnetic stirring and heating plates were utilized, one for the air seeding and one for the fuel seeding, the third and final particle seeding bottle used for the ambient surrounding particles did not require a stirring mechanism due to sufficient particle transport. The setup is represented in the scheme of Figure 5.

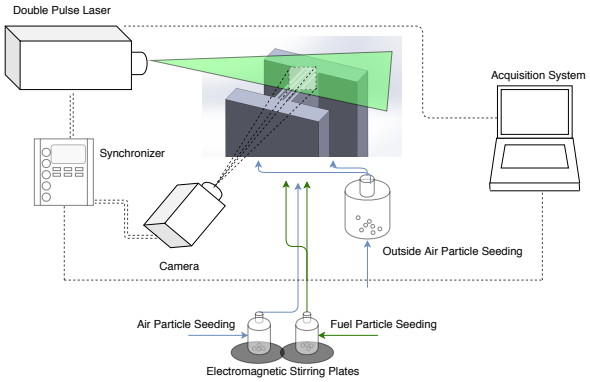

Figure 5: PIV Schematic.

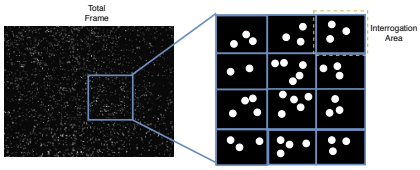

Figure 6: Interrogation Areas subdivision schematic.

Parameter	Option
Image pairs per recording	200
IA size	32x64 / 64x128
Time between pulses	60 µs / 200 µs
Correlation technique	Average Correlation
Overlapping factor	50% x 50%

Table 1: Summary of PIV parameters

Post-Processing

The second essential part of the PIV technique is the image analysis. There are a number of procedures that can be done both pre- and post-correlating the acquired particle image pairings. No pre-correlation image filtering was applied, only image masking to limit the area of interest for the analysis.

In regards to correlation methods, there are multiple approaches with different characteristics that better adapt to various kinds of flows and seeding conditions [13, 15]. Cross-correlation is a technique that calculates a 2-D velocity field from an image pair, it is a spatially statistic technique particularly well suited to flow fields with a dominant direction. This approach correlates the light intensity emitted by the particles at the instant of the first exposure (instant t) to the second exposure (instant $t + \Delta t$), in sequence the most probably displacement can be obtained through a peak detection method.

Another possible approach is "Average Correlation", where the correlation function of each interrogation area is averaged at each location for all the images. This technique is useful in applications where it can be difficult to maintain a stable particle density during the entirety of the acquisition period, which was the case with the low velocity ambient particles surrounding the slit flows.

Another important correlation parameter is the Interrogation Area (IA), which determines the subdivisions of the main frame into n x n pixels windows as shown in Figure 6. The chosen dimensions for the IA are linked to the time interval between laser pulses and the distance traveled by the particles during this time window. The three parameters must be such that a clear movement of the particles can be obtained between both frames.

3. Results

3.1. Flame Morphology

As with normal diffusion flames (NDF), the visual appearance, both in terms of structure and luminosity, of IDF is dependent on the stoichiometry, flow velocity fields of fuel and air, burner geometry and fuel type [1]. To gain insight into the working range, stabilization mechanisms and flow interactions of the IDF in a multi-slit burner, it was important to discern the effects of each parameter, therefore two different fuel flow rates, and respective flame powers, were fixed. Isolating in this way the effects of the velocity ratio, V_r (through the increase of air flow rate) and consequently the global equivalence ratio (ϕ_g) variation.

Between both flame powers, four distinct types were visualized across the entirety of the range tested: Type I is characterized by the triangular shape of the flame front; Type II presents a transition structure, where an inner flame front is generated but a disconnect is maintained with the outside flame fronts; Type III is characterized by the continuous symmetric flame fronts separated by the air jet, and finally Type IV, where the interior flame fronts rise and stabilize in a "neck-like" structure. Let us now proceed with a more in-depth analysis of each flame type. For illustrative purposes, the three independent channels are represented with colored arrows in all pictures with green corresponding to fuel flow and blue to the central air flow.

The overlay superposition of all four flame type flame fronts is presented in Figure 7

As a single representative flame, Type IV will now be presented in depth for all three experimental technique analysis.

Flame Type IV

The fourth and last flame type identified in the more extreme lean range of $0.4 \geq \phi_g \geq 0.2$, is characterized by the return to a configuration without interior attached flame fronts. These have risen to form a "neck-like" structure at the flame top, split by

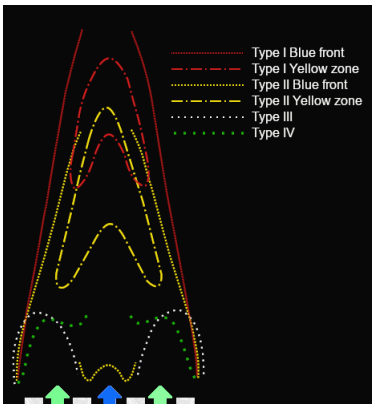

Figure 7: Combined flame front overlay.

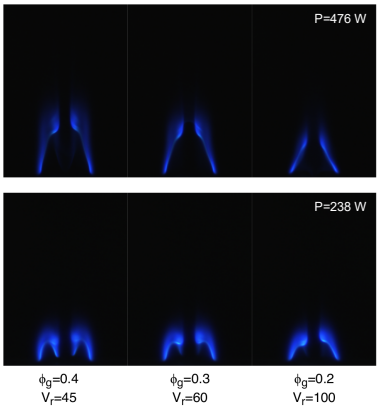

Figure 8: Type IV flame range.

the high velocity air jet, with a $V_r \geq 45$. This neck structure generation was identified by Dong et al. for a CAP burner to be triggered for $Re_{air} = 300$ [16]. Let us now, for comparative purposes, utilize the Reynolds number formula described in the previous chapter with the slot width as a reference dimension. With this definition the equivalent transition occurs at $Re_{air} = 355$ for the 238 W flame and about $Re_{air} = 450$ for the 476 W one, thus it can be concluded that for these two burner geometries the formation of a neck-like structure was present at approximate Reynolds numbers, with a slight delay for the higher powered flame. It is important to note the slight blue zone delineated by yellow stroked line in Figure 9 is a superposition of a slight flame front downward deflection occurring at the slit half span.

A highly luminous intense reaction zone can be observed in the neck curvature. Analyzing the work previously developed utilizing CAP burners, it was observed that the increase in the air Reynolds number, and consequently V_r, led to increased entrainment of the outer fuel jets into the inner air jet due to a larger pressure gradient. This phenomenon produced approaches a cross flow, forming a structure described as a flame "neck", which functioned as a mixer and holder for the upper flame torch for these burner types [3, 17, 18]. Sze et al. [19] has also reported this zone as reaching the highest temperature, indicating that the most intense combustion occurred in this part of the flame. Associating these previous observations with the knowledge that the OH concentration reaches a maximum near the position of maximum temperature [2], the intensely reactive blue neck region found in the flame type under study, can be considered as an analog to the neck constrainment found in CAP burner IDF.

This flame type is characteristic of a momentum-controlled flame, being that the main difference between this type of IDF and a buoyancy-driven partially mixed IDF is the absence of an inner flame layer [18]. For this and the Type III case, no inner flame layer is attached to the air jet exit. This is due to the increased quench effect of the cold air jet when Re_{air} and equivalently the air flow rate is sufficiently high [16, 20].

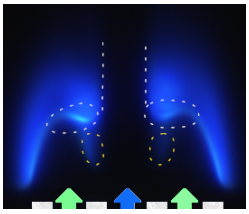

Figure 9: Type IV flame interest zones ($\phi_g = 0.3$; $V_r = 60$; $P = 238W$).

3.2. Flame Chemiluminescence

As a preliminary approach, before proceeding with the local spectroscopy, the three reference flames were analyzed utilizing a non-intrusive technique based on the processing of flame images acquired with a charged coupled device (CCD) camera utilizing an equivalence ratio analysis algorithm, developed in-house. This analysis provided a comparative reference for the chemiluminescence spectroscopy and as a case-study for the validation of the numerical algorithm.

3.2.1 Type IV

The following results were obtained for the Type IV flame ($\phi_g = 0.3$; $V_r = 60$)

For this third and final case, the numerical algorithm detected the entirety of the flame front, with a clear local equivalence ratio gradient. As expected for a diffusion flame, the existence of a zone presenting close to stoichiometric conditions, is clear. This thin zone is surrounded by an interior rich zone (red color) on the fuel jet side, and a lean zone (blue color) on the ambient air side.

The most notable result for this flame type is the presence of the most fuel rich region at the concave side of the neck contraction, indicating a fuel accumulation at that same region. This could be indicative of a recirculative phenomenon, which will

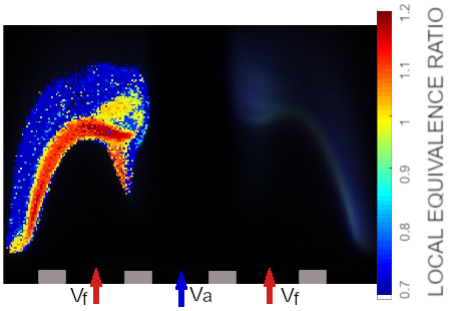

Figure 10: Local equivalence ratio results of flame Type IV ; ($\phi_g = 0.3$; $V_r = 60$; $P = 238W$).

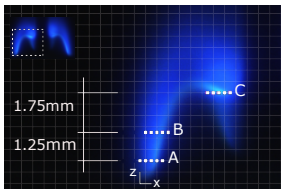

(a) Spectroscopy acquisition positioning detailed view

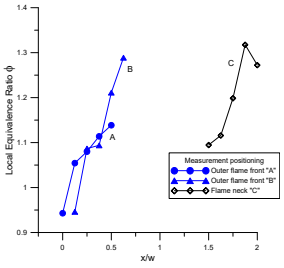

(b) Combined measurements

Figure 11: Type IV ($\phi_g = 0.3$) spectroscopy results.

be further investigated utilizing the particle image velocimetry (PIV).

3.3. Local Spectroscopy

Based on the preliminary image processing analysis three interest zones were established for the different flame morphologies, with an additional fourth zone for the Type II flame at the interior flame structure coupled to the central air slit. For each region, five acquisition points were established traversing the flame front with steps of 0.25 mm. These are displayed in the images coupled with a positioning grid, adjacently, the complete local equivalence ratio (ϕ) results for each flame type are represented with horizontal positioning adimensionalized by slot width "w".

Analyzing Figure 11, there is once again a generalized tendency in ϕ increase for corresponding positions at different heights for the outside flame front, but with no ϕ value inversion for the most interior points as seen in Type III. This is indicative of the existence of a mechanism impeding the free impingement of the fuel flow towards the central air jet, which would expectantly be greater due to a more intense velocity gradient for this last case ($V_r = 60$). The indication of such phenomenon could already be observed in the image processing results, through the presence of a rich zone in the curvature at the neck attachment.

Focusing on the neck attachment zone, the increased fuel presence ascertained from the image processing results is confirmed, there is a point of maximum ϕ located in this zone, pointing towards the possible existence of a fuel recirculation, defining this as an interest zone for the PIV analysis.

3.4. PIV Analysis

3.4.1 Type IV

Observing the vector map (Figure 12), the fuel flows are seen to start impinging the central air jet immediately after the burner exit (before the flame base). After this mixture and momentum exchange, there is an outwards movement as the particles cross the intensely reacting neck constrainment region. Bearing in mind the high fuel concentration previously detected in this region, using the numerical ϕ assessment algorithm and confirmed through the local spectroscopy, a further IA dimension refinement was applied to this region of interest. The laser pulse interval utilized in the previous analysis was maintained but the IA was reduced to 16x32 pixels in order to accurately measure the more intricate details of the particle movements in the region of interest, which can be lost when utilizing an inadequate IA sizing or pulse interval, as described in sub-section 2.2.

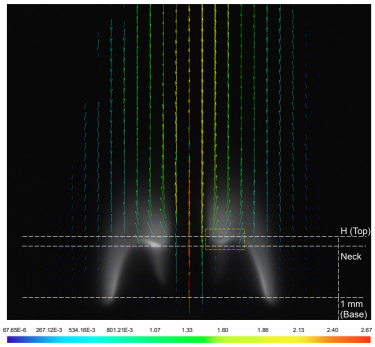

Figure 12: Type IV vector mapping ($\Delta t = 200ms; \phi_g = 0.3$). Detailed view location delineated by yellow dashed line.

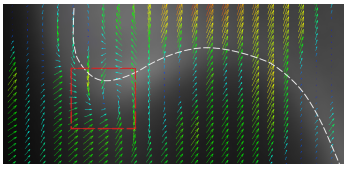

Figure 13: Type IV Neck vector mapping detailed view ($\Delta t = 200ms; IA = 16 \times 32px; \phi_g = 0.3$).

Figure 13 presents the region of interest with the flame front centerline delineated in dashed line as a visualization aid. The refined analysis detected a flow recirculation zone at the neck con-

strainment (red dashed highlight region). The neck region has been observed in a number of studies as previously mentioned, but a flow reversal and recirculation in this region has seldom been reported. Elbaz et al. [21] found neck flow reversal regions for singular very specific flow condition ($V_r = 20.7; Re_{air} = 2500$) in a co-annular (CoA) burner. This was associated with poor mixing as the fuel jets are deflected outwards and resulted in the generation of an outer yellow soot ring. For the present analysis, although the Reynolds number is inferior ($Re_{air} = 1185$), the velocity ratio is substantially greater ($V_r = 100$) and there is no apparent generation of a yellow soot-producing region. In fact, the flame is decreasing in height towards this regime, indicating an even more intense mixing happening in the air-fuel jet interfaces [16, 17, 21]. Therefore, the flow reversion phenomenon found by Elbaz et al. in the neck region does not seem to be correlated with the case under study.

Delving further into the analysis of this flow recirculation region, the work developed by Dong et al. [18] with a circumferential arranged ported (CAP) burner, found a much more prevalent range of IDFs with a neck constrainment region. As Re_{air} exceeded 300, the recirculation zone was seen to be present and this region was maintained up to flame blowoff. Therefore, the present findings show a much better correlation to the results of Dong et al. for the CAP burner, with the increasing V_r aggravating fuel jets impingement acting as cross-flows for the central air jet. The high pressure formed around the impingement stagnation point creates a recirculation zone, functioning as a structural stabilization aid mechanism at the flame neck. The stabilization effect of this impingement-induced recirculation zone is proved to be very effective in guaranteeing an extremely globally lean range of flame operating conditions.

In regards to the isothermal and flame velocity profile comparison, once again the velocity increase is evident, in particular for the outer fuel flows as well as the outside air entrainment. For the velocity profile development, a main detail can be observed for this flame morphology. In contrast to the velocity increase for the outer flows, due to the presence of the flame front, the central air jet velocity diminishes downstream along the central line. This is to be expected due to the structure of the flame "neck". Some of the air will progress downstream without participating in the flame front combustion, thus naturally shedding velocity by momentum transfer to the surroundings. This results in the highest air slit center line velocity being measured at the burner exit, and the lowest at the flame top (as can be seen in Figure 14(b)).

It is relevant to note that for the Type III flame,

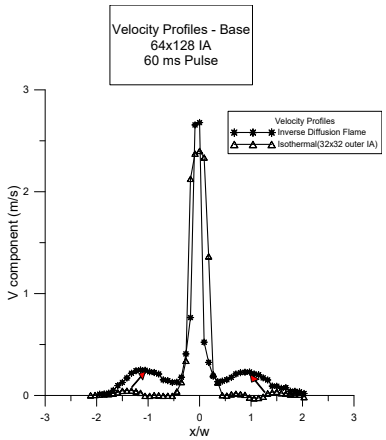

(a) Isothermal and Flame velocity profiles.

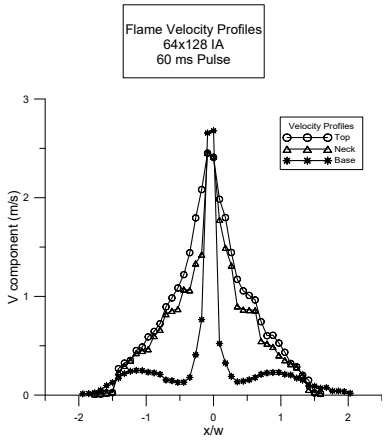

(b) Profile development downstream.

Figure 14: Isothermal comparison and flame velocity profile development ; $\phi_g = 0.3$.

the central air vertical pathway was also clear of any flame region. However, Type IV does not possess the two interior flame fronts adjacent to the air jet increasing the central jet velocity due to the momentum transfer from the hot accelerated combustion products exiting in normal direction from the flame front and the pre-heating effect caused by flame heat conduction and radiation.

3.5. Morphological analysis overview

In summary, each of the three techniques, utilized with the goal of characterizing the IDF multi-slot burner morphologies, provided an important input in understanding the working mechanisms of the flames. The fuel and air flow interactions visualized with the particle image velocimetry together with the measurements of local equivalence ratio (ϕ) values provided a fundamental view into how the various flame structures, observed initially through the flame photography, react to the alterations in velocity ratio (V_r). To further illustrate the mechanisms characteristic to each flame type, a condensed flame

schematic is presented in Figure 15 for each of the three flame types (and respective global equivalence ratio (ϕ_g) ranges), II, III and IV studied in depth experimentally.

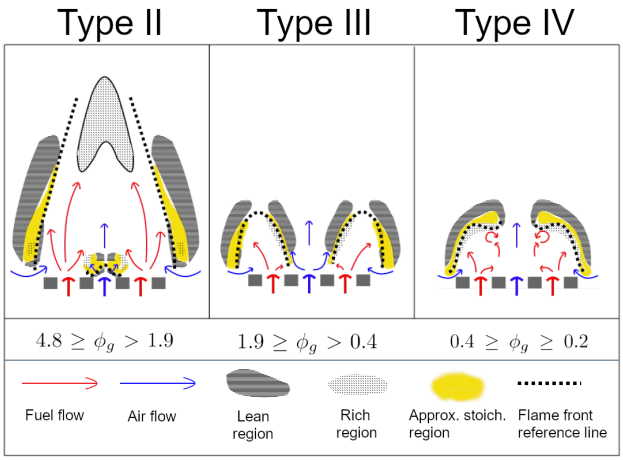

Figure 15: Condensed flame type schematic.

4. Conclusions

A summary of the most important findings of this thesis is itemized below:

1. Four distinct methane IDF flame types for the complete working range of the multi-slot burner were identified: Type I characterized by the triangular shape of the flame front with a clear yellow soot production zone; Type II presenting a transition structure, where an inner flame front is generated but a disconnect is maintained with the outside flame fronts; Type III characterized by the continuous symmetric flame fronts separated by the air jet and the absence of any yellow soot producing zone, and finally Type IV, where the interior flame fronts rise and stabilize in a "neck-like" structure with a completely blue flame and no visible soot production.

2. It was verified that the lean blowout limit is not affected by the fuel flow rate, as previously shown by Zhang et al. for a CoA burner [22].

3. The velocity ratio (V_r) was found to be an important governing parameter in the definition of the flame structures, This is due to its role in the air-fuel jet entrainment. The shear forces and pressure gradients generated between jets, through the V_r increase, intensify the inter-jet mixing, increasing the local reaction rates and shortening the visual flame height.

4. The formation of the neck-like structure was found to occur at $Re_{air} = 355$ for the 238 W flame and $Re_{air} = 450$ for the 476 W one, which are in agreement with the results for CAP burners [16].

5. The sudden visual flame height reduction occurring at the transition to flame Type III was detected at $V_r = 10$ which compared to the previously reported value of $V_r = 15$ at the moment of a substantial height reduction for CoA burner [21], shows a quite good accordance.

6. Through the measurement of the local equivalence ratio (ϕ), it was possible to detect a clear contrast between the interior and exterior flame fronts for flame Type III. Presenting a more significant fuel presence towards the interior flame front, which is indicative of the fuel flow movement towards the high velocity air jet. A similar movement of fuel was detected for Type II, with the formation of a richer zone at the smaller central flame front.

7. For flame Type IV, through the chemiluminescence spectroscopy, a rich area was detected at the neck constrainment region, indicating a possible recirculation phenomenon. This was verified through the velocity vector mapping obtained with the particle image velocimetry (PIV) technique. The high pressure formed around the impingement stagnation point creates a recirculation zone, functioning as a structural stabilization aid mechanism at the flame neck. The stabilization effect of this impingement-induced recirculation zone is proved to be very effective in guaranteeing an extremely globally lean range of flame operating conditions.

Acknowledgements

I would like to thank Professor Edgar Fernandes not only for all the support and motivation during this thesis, but also the enthusiasm with which his courses are lectured, which, in truth, motivated me in approaching this interesting topic.

A special acknowledgment goes to Filipe Quintino for the immeasurable support and availability during the course of this thesis, the help provided was invaluable in reaching the goals of this work.

To all my laboratory colleagues and specially João Xavier, Rui Araújo and André Korolev for the companionship along this journey.

Finally to Renata Rodrigues and my family to which I dedicate this work.

References

[1] Kuang-Tsai Wu and Robert H. Essenhigh. Mapping and structure of inverse diffusion flames of methane. *Symposium (International) on Combustion*, 20(1):1925–1932, jan 1985.

[2] M Mikofski, T Williams, C Shaddix, A Fernandezpello, and L Blevins. Structure of laminar sooting inverse diffusion flames. *Combustion and Flame*, 149(4):463–478, jun 2007.

[3] J Miao, C.W. Leung, C.s Cheung, and Randolph Leung. Flame stability and structure of liquefied petroleum gas-fired inverse diffusion flame with hydrogen enrichment. *Word Acad Sci*, pages 720–725, 01 2012.

[4] Christopher R. Shaddix, Timothy C. Williams, Linda G. Blevins, and Robert W. Schefer. Flame structure of steady and pulsed sooting inverse jet diffusion flames. *Proceedings of the Combustion Institute*, 30(1):1501–1508, jan 2005.

[5] A.M. Elbaz and W.L. Roberts. Flame structure of methane inverse diffusion flame. *Experimental Thermal and Fluid Science*, 56:23–32, jul 2014.

[6] D. P. Mishra. *Experimental Combustion: An Introduction*. CRC Press, 2017.

[7] J. Miao, C.W. Leung, C.S. Cheung, Z.H. Huang, and H.S. Zhen. Effect of hydrogen addition on overall pollutant emissions of inverse diffusion flame. *Energy*, 104:284 – 294, 2016.

[8] Mark A. Mikofski, Timothy C. Williams, Christopher R. Shaddix, and Linda G. Blevins. Flame height measurement of laminar inverse diffusion flames. *Combustion and Flame*, 146(1):63 – 72, 2006.

[9] S. Mahesh and D.P. Mishra. Flame structure of LPG-air inverse diffusion flame in a backstep burner. *Fuel*, 89(8):2145–2148, aug 2010.

[10] L.K. Sze, C.S. Cheung, and C.W. Leung. Appearance, temperature, and NOx emission of two inverse diffusion flames with different port design. *Combustion and Flame*, 144(1-2):237–248, jan 2006.

[11] A. G. Gaydon. Flame spectrophotometry. In *The Spectroscopy of Flames*, pages 320–337. Springer Netherlands, 1974.

[12] Teodoro Trindade, Artur Ferreira, and Edgar Fernandes. Characterization of combustion chemiluminescence: An image processing approach. *Procedia Technology*, 17:194–201, 2014.

[13] R Bastiaans. Cross-correlation piv : theory, implementation and accuracy. *Compustion Technology*, 4, 01 2000.

[14] K Okamoto, S Nishio, T Saga, and T Kobayashi. Standard images for particle-image velocimetry. *Measurement Science and Technology*, 11(6):685–691, may 2000.

[15] C Brossard, J.-C Monnier, P BARRICAU, F.X. Vandernoot, Yves Le Sant, Frederic Champagnat, and Guy Le Besnerais. Principles and applications of particle image velocimetry. 1, 2009.

[16] L.L. Dong, C.S. Cheung, and C.W. Leung. Heat transfer characteristics of an impinging inverse diffusion flame jet. part II: Impinging flame structure and impingement heat transfer. *International Journal of Heat and Mass Transfer*, 50(25-26):5124–5138, dec 2007.

[17] L.L. Dong, C.S. Cheung, and C.W. Leung. Combustion optimization of a port-array inverse diffusion flame jet. *Energy*, 36(5):2834 – 2846, 2011.

[18] L.L. Dong, C.S. Cheung, and C.W. Leung. Heat transfer characteristics of an impinging inverse diffusion flame jet – part i: Free flame structure. *International Journal of Heat and Mass Transfer*, 50(25-26):5108–5123, dec 2007.

[19] L.K Sze, C.S Cheung, and C.W Leung. Temperature distribution and heat transfer characteristics of an inverse diffusion flame with circumferentially arranged fuel ports. *International Journal of Heat and Mass Transfer*, 47(14-16):3119–3129, jul 2004.

[20] Andrzej Sobiesiak and Jamie C. Wenzell. Characteristics and structure of inverse flames of natural gas. *Proceedings of the Combustion Institute*, 30(1):743–749, jan 2005.

[21] A. M. Elbaz and W. L. Roberts. Experimental characterization of methane inverse diffusion flame. *Combustion Science and Technology*, 186(9):1249–1272, 2014.

[22] Yi Zhang and Peter B. Sunderland. Quenching limits of inverse diffusion flames with enriched oxygen. *Combustion and Flame*, 162(6):2743–2745, jun 2015.